Journal of Alloys and Compounds 509 (2011) 3367–3374

Contents lists available at ScienceDirect

Journal of Alloys and Compounds

journal homepage: www.elsevier.com/locate/jallcom

Hierarchical CuO hollow microspheres: Controlled synthesis for enhanced lithium storage performance

Xiangfeng Guan [a], Liping Li [b], Guangshe Li [a,*], Zhengwei Fu [a], Jing Zheng [b], Tingjiang Yan [a]

[a] State Key Laboratory of Structural Chemistry, Chinese Academy of Sciences, Fuzhou 350002, PR China
[b] Key Laboratory of Optoelectronic Materials Chemistry and Physics, Chinese Academy of Sciences, Fuzhou 350002, PR China

ARTICLE INFO

Article history:
Received 27 September 2010
Received in revised form 9 December 2010
Accepted 9 December 2010
Available online 21 December 2010

Keywords:
Oxide materials
Chemical synthesis
Microstructure
X-ray diffraction
Transmission electron microscopy
Electrochemical behavior

ABSTRACT

In this work, hierarchical CuO hollow microspheres were hydrothermally prepared without use of any surfactants or templates. By controlling the formation reaction conditions and monitoring the relevant reaction processes using time-dependent experiments, it is demonstrated that hierarchical CuO microspheres with hollow interiors were formed through self-wrapping of a single layer of radically oriented CuO nanorods, and that hierarchical spheres could be tuned to show different morphologies and microstructures. As a consequence, the formation mechanism was proposed to proceed via a combined process of self-assembly and Ostwald's ripening. Further, these hollow microspheres were initiated as the anode material in lithium ion batteries, which showed excellent cycle performance and enhanced lithium storage capacity, most likely because of the synergetic effect of small diffusion lengths in building blocks of nanorods and proper void space that buffers the volume expansion. The strategy reported in this work is reproducible, which may help to significantly improve the electrochemical performance of transition metal oxide-based anode materials via designing the hollow structures necessary for developing lithium ion batteries and the relevant technologies.

1. Introduction

Copper oxide (CuO), a p-type semiconductor with a narrow band gap of about 1.2 eV, has been widely exploited for a versatile range of applications, such as catalysis [1], lithium ion electrode materials [2], solar cells [3], and magnetic storage media [4]. Among all these potential applications, the use of CuO as the anode materials for next generation rechargeable lithium-ion batteries (LIBs) has been intensively studied because of high theoretical capacity, high safety, environmental benignity, and low cost [5]. For instance, when used as the anode material, a conversion mechanism is expected [6]:

$$CuO + 2Li^+ \leftrightarrow Li_2O + Cu\text{–}2e \quad (1)$$

Based on a maximum uptake of 2 Li per CuO, the theoretical capacity [7] for CuO is calculated to be 670 mAh g^{-1}, which is much higher than that of 372 mAh g^{-1} for conventional graphite. These electrochemical performances could be further improved when made into nanoscale as for many nanostructured materials because of the size effects [8,9]. As a result, many great efforts have been done to prepare various types of CuO nanostructures which include nanoparticles (0D) [10], nanowires [11], nanorods (1D) [12], nanosheets (2D) [13], and 3D hollow nanostructures [14] with an aim to achieve the optimized electrochemical performance of CuO. In spite of much progress in this regard, as for other nanoscale metal oxides, the practical applications of CuO nanostructures are still hampered by a drastic change in specific volume of about 80% during the Li uptake/release processes [15], leading to the pulverization problem and moreover a rapid deterioration in capacity [16]. Therefore, as a case study, it is fundamentally important to develop a new strategy that can accommodate CuO nanostructures with sufficient spaces to sustain the volume change from Li^+ uptake and release, which may provide useful hints for many types of oxide nanostructures to find applications in high performance lithium-ion batteries.

Synthesis of 3D hierarchical microspheres with hollow interiors can be a best option for this purpose, since one can take the advantages of the merits of each sub-structures [17–20], which include the nanometer-sized building blocks, hollow interiors, and micrometer-sized spherical assemblies [21]. For instance, nanometer-sized building blocks may provide high surface areas for high capacity, hollow interiors are favourable for improving the structural stability by sustaining the volume change during the Li^+ uptake/release processes, and spherical assemblies could guarantee the high stacking density. Further, once the hollow microspheres were constructed by assembly of nanorods, the transport of lithium-ions can be accelerated, as reported in certain systems [22]. Therefore, synthesis of CuO that posses this kind of hierarchical hollow structures is highly attractive and becomes an

* Corresponding author. Tel.: +86 591 83702122; fax: +86 591 83702122.
E-mail address: guangshe@fjirsm.ac.cn (G. Li).

0925-8388/$ – see front matter © 2010 Elsevier B.V. All rights reserved.
doi:10.1016/j.jallcom.2010.12.067

important issue to be addressed in this work. Unfortunately, as for majority of oxide nanomaterials, controlled organization into hollow spherical structure from rod-like building blocks still remains as a challenge [23].

The most difficulties in synthesizing hollow nanostructures are represented by the use of templates, hard or soft, to guide the formation of outer shells. Although the template methods have been proven very effective and versatile for synthesizing various hollow structures, the required toxic raw materials, the removal of the template and the contamination of by-products limit their exploitation at the application level [24]. Herein, we demonstrate a controlled green method based on Ostwald's ripening for synthesizing hierarchical hollow microspheres assembled with CuO nanorods simply using $Cu(CH_3COO)_2{\cdot}H_2O$ as the starting material instead of any toxic and dangerous reagents, such as ammonia solution [2] and sodium hydrate [25]. Depending on the reaction condition, hierarchical microspheres were tuned to show different morphologies and microstructures. When explored as the anode materials for lithium ion batteries, CuO hollow microspheres showed excellent cycle performance and enhanced lithium storage capacity. This superior cyclic stability and high capacity are beneficial from the synergetic effect of small diffusion lengths in nanorod building blocks and proper void space that buffers the volume expansion.

2. Experimental

2.1. Sample synthesis

Hierarchical CuO architectures were prepared by a hydrothermal method using $Cu(CH_3COO)_2{\cdot}H_2O$ as the copper source. In a typical procedure, a given quantity (1.36 g) of $Cu(CH_3COO)_2{\cdot}H_2O$ was added into 68 ml of deionized water to form a transparent blue solution. The obtained solution was transferred to 100 ml Teflon-lined stainless steel autoclaves, which were allowed to react at 120 °C for 24 h and then cooled naturally to room temperature. The resulting black solid product was filtered, washed several times with distilled water, and then vacuum-dried at 150 °C.

2.2. Sample characterization

Phase structures of the samples were characterized by X-ray diffraction (XRD) on a Rigaku MiniFlex II X-ray diffractometer using a copper target. Sample morphologies were determined using field emission scanning electron microscopy (FE-SEM) on a JEOL JSM-6700 apparatus and transmission electron microscopy (TEM) on a JEM-2010 apparatus with an acceleration voltage of 200 kV. Samples for TEM measurements were prepared by making a dispersion of the samples in ethanol and putting drops of them on a carbon-coated copper grid.

2.3. Electrochemical characterization

Electrochemical characterizations of the samples were performed using CR2025 coin-type cell. The anode materials were fabricated by mixing the as-prepared CuO powders, acetylene black, and PVDF at weight ratios of 60:20:20, respectively, using N-methylpyrrolidone (NMP) as a solvent. The resulting slurries were uniformly coated onto the copper foil by a doctor blade technique. After coating, the film was dried at 100 °C under vacuum for 10 h. CR2025 coin-type cell were assembled in an argon-filled glove box (H_2O and O_2 concentration <1 ppm) using a metal lithium foil as the counter electrode, 1 M $LiPF_6$ in EC:EMC:DMC (1:1:1 in volume) as electrolyte and porous polypropylene film as separator. The cells were charged and discharged galvanostatically using a battery tester (Land Battery Test System) in the voltage range between 0.01 and 3.0 V.

3. Results and discussion

The crystallographic structures of the samples were examined by X-ray diffraction (XRD). Fig. 1 shows the XRD pattern of the sample obtained after reaction at 120 °C for 24 h. All diffraction peaks can be assigned to the monoclinic structure for CuO (JCPDS card no. 80-1268, space group: $C2/c$, $a = 4.683$ Å, $b = 3.421$ Å, $c = 5.129$ Å, $\beta = 99.57°$). No other diffraction peaks were observed, which indicate the high phase purity. The strong and broad XRD peaks in Fig. 1 also indicate that the as-prepared sample was composed of nanocrystallites. Using the Scherrer formula for the (2 0 2) diffraction peak of CuO, the average crystallite size was calculated to be

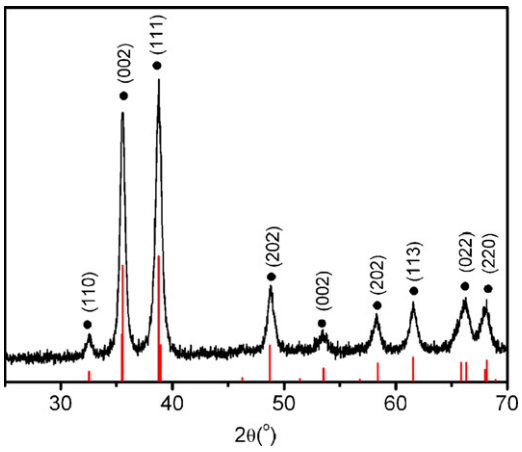

Fig. 1. XRD pattern for the sample obtained after hydrothermal reaction at 120 °C for 24 h. Vertical bars represent the standard diffraction data for CuO from JCPDS card no. 80-1268.

9.8 nm, which confirmed the nanocrystalline nature of as-prepared sample.

Morphologies and microstructures of the as-prepared samples were examined by FE-SEM. Typical FESEM images of the samples at different magnifications are shown in Fig. 2. The panoramic image of the as-prepared sample in Fig. 2a clearly indicates that the as-prepared CuO was microspheres with an average diameter of about 3.5 μm, showing a high-yield growth and good sample uniformity of CuO superstructures. As shown by the magnified image in Fig. 2b and c, the surfaces of the microspheres were rough and composed of numerous nanoparticles. Therefore, CuO microspheres were assembled by nanosized crystallites. Further FE-SEM image of a single broken sphere clearly reveals that the entire architectures for microspheres were constructed by a single layer of oriented nanorods which were self-wrapped to form the hollow interiors with an average diameter of 1 μm (Fig. 2d).

To get insights into the micro-structural details, CuO microsphere samples were carefully ground and ultra-sonicated in ethanol, and further examined by TEM in combination with selected area electron diffraction (SEAD). A typical TEM image of a broken piece of CuO microsphere was illustrated in Fig. 3a, which confirms that CuO microspheres were assembled by a large quantity of oriented nanorods which are aligned perpendicularly to the sphere surfaces, pointing outwards from the common inner center. Along the growth direction, the oriented assembled nanorods gradually increased in width from 5 to 20 nm. Due to the orientation difference between these nanorods, quantities of nanoscale cavities existed within the shell of CuO microspheres. For a shell fragment (Fig. 3b), high-resolution TEM image indicates the distinct lattice fringes with a spacing of 0.23 nm (Fig. 3c), which is corresponding to the (1 1 1) plane of the monoclinic CuO. Selected area electron diffraction (SAED) pattern dots (Fig. 3d) were aligned as 2D arrays but these diffraction spots were not regularly round in shape but noticeably elongated. Therefore, all oriented nanorods that constructed CuO hollow microspheres were tiny single crystals with similarly preferential orientation along the [0 2 1] direction and the neighboring individual nanorods were assembled roughly parallel, showing a very small tilt angle. Further, SAED in Fig. 3e confirms that the individual elongated CuO crystallites were single-crystalline with the primary axes pointing along the direction [0 2 1] of the crystal.

Many kinds of hierarchical hollow structures of CuO have already been reported in the literature. For example, Wan and co-workers [2] have prepared CuO hollow spheres assembled by nanoplates using a soft template method, in which hollow struc-

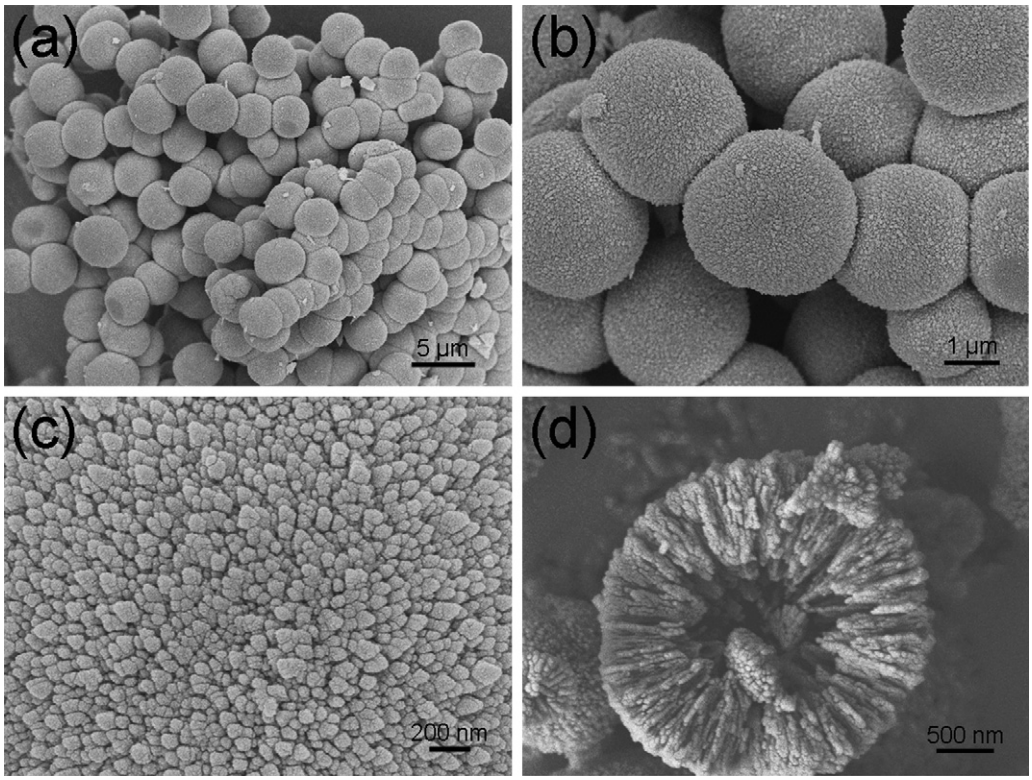

Fig. 2. FE-SEM images of the CuO microspheres prepared at 120 °C for 24 h: (a) overall morphology; (b) low-magnification FESEM image of microspheres; (c) high-magnification FESEM image of the surface of a single sphere; and (d) a cracked sphere that shows the hollow interior.

ture is formed via the directing role of P123 spherical micelles in solution. Jiang and co-workers [5] concluded that the hierarchical CuO hollow spheres can be obtained by assembly of nanosheets with the help of tyrosine for its special structure and strong assembling functions. The common feature for these spheres is that the shell is composed of numerous nanoparticles with an irregular arrangement, which is apparently different from the microspheres assembled by nanorods reported in this work. Since there were no templates or surfactants used in this work and our hollow spheres were composed of oriented self-assembled nanorods, the formation of the present CuO hollow spheres can be different from those previously reported for spheres that were assembled by nanoparticles. To obtain a substantial view of the growth mechanism of the CuO hollow microspheres, time-dependent evolution process was monitored by FE-SEM. Fig. 4 shows the FE-SEM images of the microspheres that were obtained at 120 °C with prolonging the duration of reaction time. After 30 min reactions, irregular solid spheres with an average diameter of 600 nm were formed, showing rough surfaces (Fig. 4a). When the reaction time was increased to 2 h, the diameter of the solid spheres increased, which the surfaces became smoother (Fig. 4b). A close observation reveals that the sphere surfaces were densely covered by a great deal of small nanoparticles with a diameter of about 20 nm (Fig. 4c). Further prolonging the reaction time up to 8 h, the diameter of the solid spheres did not show apparent changes but rougher surfaces and the constituent nanoparticles grew larger to show clear edges (Fig. 4d). An

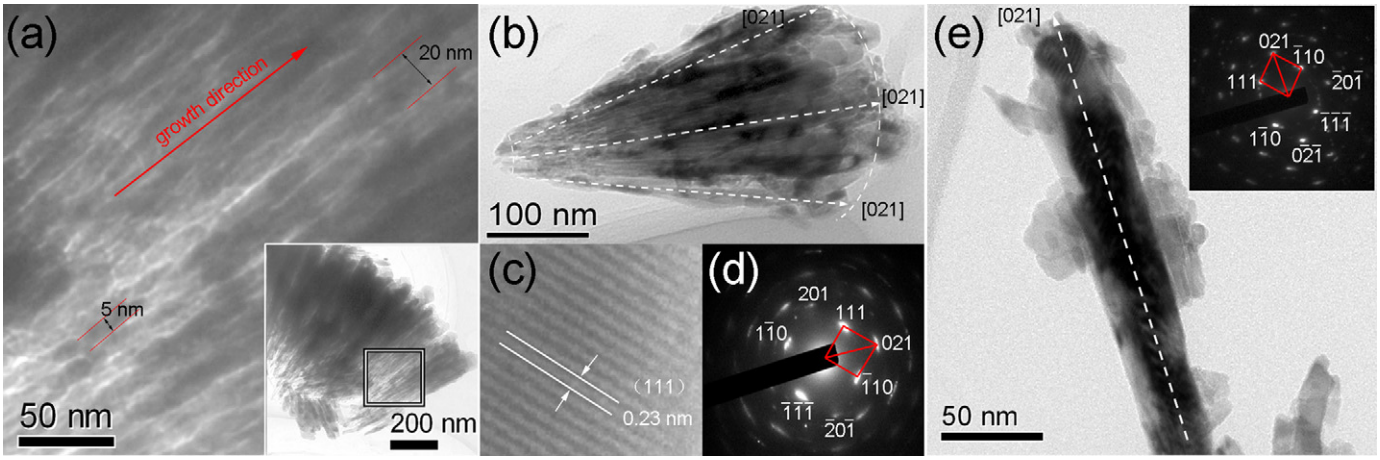

Fig. 3. (a) TEM image taken from the edge of a broken piece of the CuO hollow microsphere; (b) texture of a shell fragment; (c) HRTEM image of the singular nanorod; (d) SAED pattern of a singular nanorod; and (e) a representative TEM image and the relevant SAED of a singular CuO nanorod. Inset shows the enlarged part of the shell of CuO microsphere.

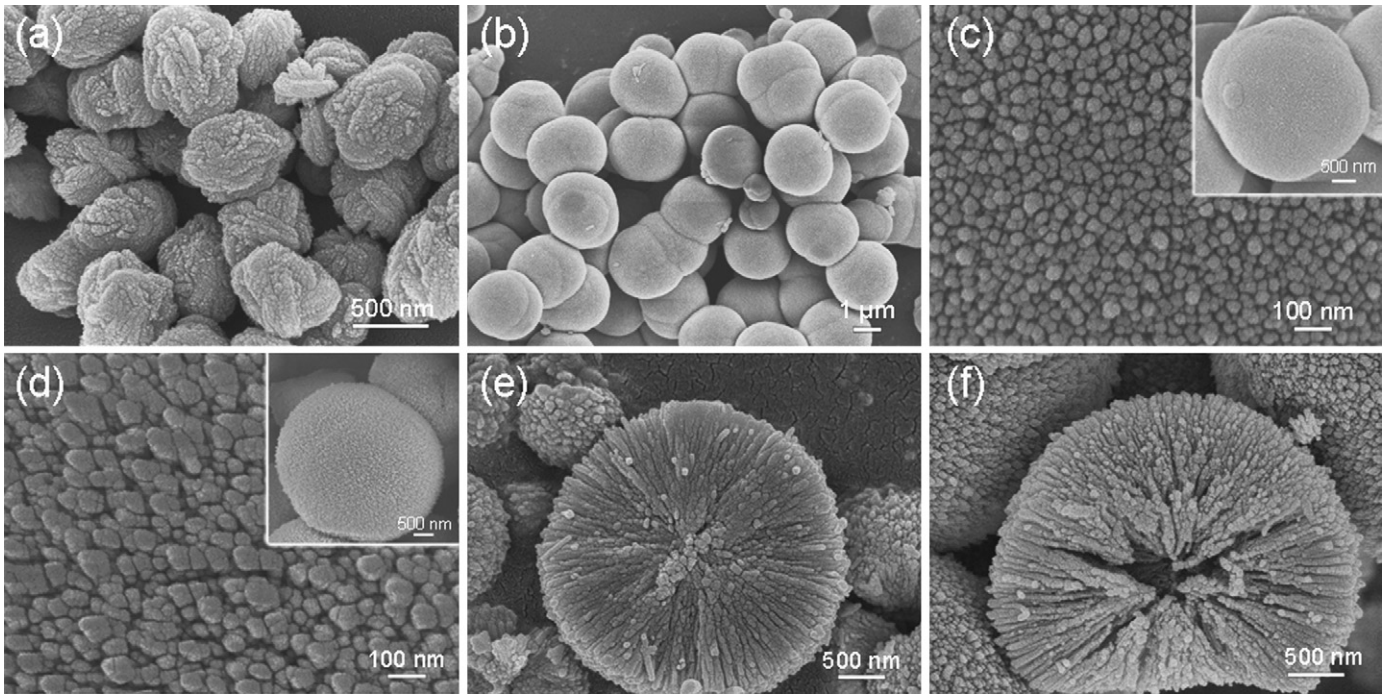

Fig. 4. FE-SEM images of CuO microspheres when the formation reaction was proceeded at 120 °C for given period of reaction time: (a) 30 min, (b and c) 2 h, (d) 4 h, (e) 8 h, and (f) 16 h.

intersection view of a singular broken sphere indicates that these microspheres are densely packed (Fig. 4e). Prolonging the reaction time to 16 h led to the hollow interiors within the microspheres (Fig. 4f). As a result, the hollow structures started to form from the interior of the aggregated particles. These aggregated spherical particles began to show thinner shells and larger hollow interior when the reaction time was increased to 24 h, as shown in Fig. 2d.

On the basis of the above experimental results, it is reasonable to presume that the formation of hollow CuO hierarchical microspheres likely proceeded via self-assembly process accompanied with Ostwald's ripening [26,27]. The whole process could be illustrated in Fig. 5. Because there were no bases added in the reaction systems, hydrolysis could be regarded as a possible pathway:

$$Cu(CH_3COO)_2 + H_2O \rightarrow CuO + 2CH_3COOH \quad (2)$$

Namely, in the first stage, tiny crystalline nuclei were generated in the supersaturated solution, which grew into nanoparticles. These primary nanoparticles might be quickly formed and further spontaneously aggregated to form spherical aggregates with minimizing interfacial energies. Subsequent grain growth is initiated preferentially from the most thermodynamically active clusters on the surface of the spherical aggregates. Owing to the supersaturated $Cu(Ac)_2$ solution surrounding the active clusters, symmetric microspheres that were assembled by singular nanorods could appear. Driven by the natural tendency of polar crystal growth in CuO, the growth fronts could radiate towards the exterior of the microspheres since the randomly oriented growth is physically limited. Because the crystallites located in the cores may have a smaller crystallite size and higher surface energies compared to those in the exteriors, the energy difference between the large particles located in the exteriors and the small particles in the cores provides the driving force for Ostwald's ripening process. Therefore, in the second stage, the Ostwald ripening process may dominate the subsequent growth of the microspheres. During this process,

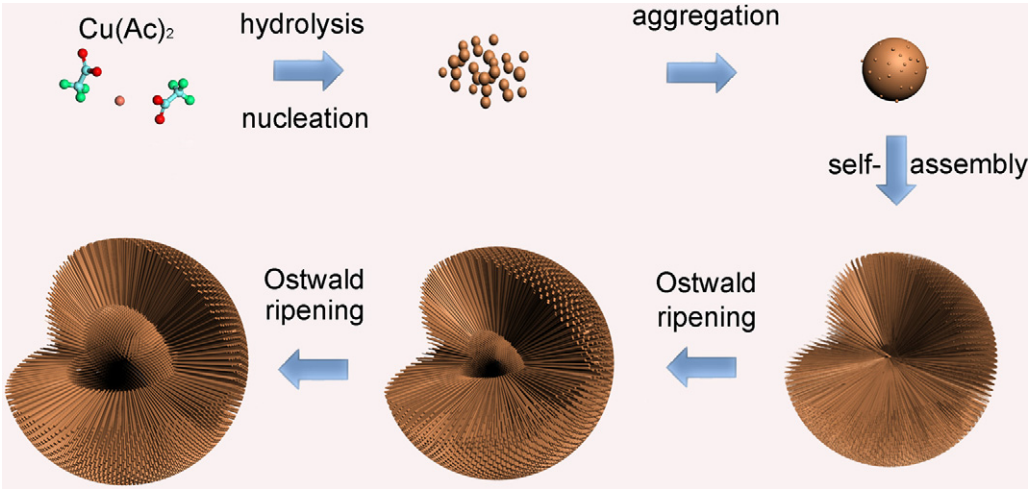

Fig. 5. Schematic illustration of the formation mechanism proposed for CuO hollow spheres.

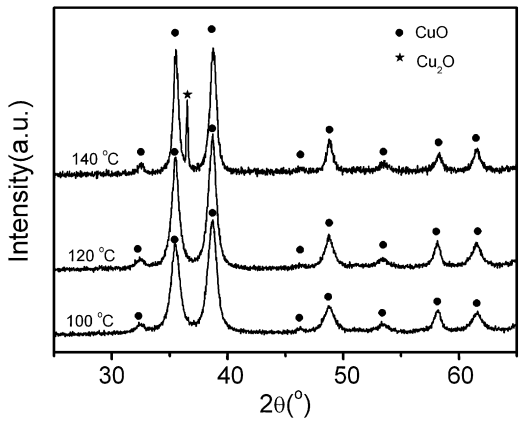

Fig. 6. XRD patterns of the samples when prepared at given temperatures for 24 h.

the crystal growth could be initiated from the most thermodynamically active particles in the cores, which serve as the crystal seeds for the subsequent recrystallization process and durative crystal growth. The particles in the cores dissolve in a direction perpendicular to the shell surface, which corresponds to a shortest distance between interior and exterior spaces. As a consequence, the outer particles become larger at the expense of the smaller particles, which results in a vacant space and thus the formation of hollow nanospheres. Due to the dynamic processes of the Ostwald ripening, there are plenty of channels available in the shell which may remain unblocked for mass transport as long as the ripening proceeds [28]. Therefore, this unique CuO hollow architecture features both boundary nanoscale cavities and hollow interior which are promising for applications as lithium ion batteries anode materials.

It is well documented that the reaction temperature plays an important role in determining the phase and morphology of the final product. Thus, the effect of reaction temperature on the formation of CuO microspheres was investigated. A series of samples were prepared after reaction at 100–140 °C for 24 h, while keeping other experimental conditions unchanged. XRD patterns of the samples are shown in Fig. 6. It can be seen that the diffraction lines of the samples when prepared at 100 and 120 °C could be indexed to a pure phase of CuO. However, when the reaction temperature was further increased to 140 °C, traces of Cu_2O were detected, which indicates that CuO phase was partially reduced to Cu_2O. Since no reductant was involved in our synthesis systems and since previous literatures have reported that acetic acid can act as a weak reducing agent [29], we believe that the by-product of CH_3COOH in Reaction (2) resulted in the formation of Cu_2O phase at temperatures above 120 °C. Using the Scherrer formula for the (2 0 2) diffraction peak of CuO, the average crystallite sizes of the samples made under different hydrothermal temperatures were calculated. It was found that with hydrothermal temperature increasing from 100 to 140 °C, the average crystallite sizes of CuO increase from 8.2 to 13.5 nm. For the sample prepared at 140 °C, the average crystallite size of Cu_2O is calculated to be 51.1 nm. It is thus confirmed that all samples are composed of nanocrystals.

FE-SEM images were used to monitor the morphology evolution as a function of reaction temperature. As shown in Fig. 7, the dominant products at 100 °C were composed of aggregated irregular microspheres with a diameter of about 3 μm. This is attributed to the slow diffusion at lower temperatures. From the magnified FE-SEM image (inset of Fig. 7a), it is clear that the microsphere was constructed by lots of nanoparticles. The dense structure was resolved from a cracked sphere (inset in Fig. 7a). When the reaction temperature was increased to 120 °C, the dimension of the spheres was nearly the same, while the dimension of the smaller particles became larger, showing hollow interior (Fig. 2b and d).

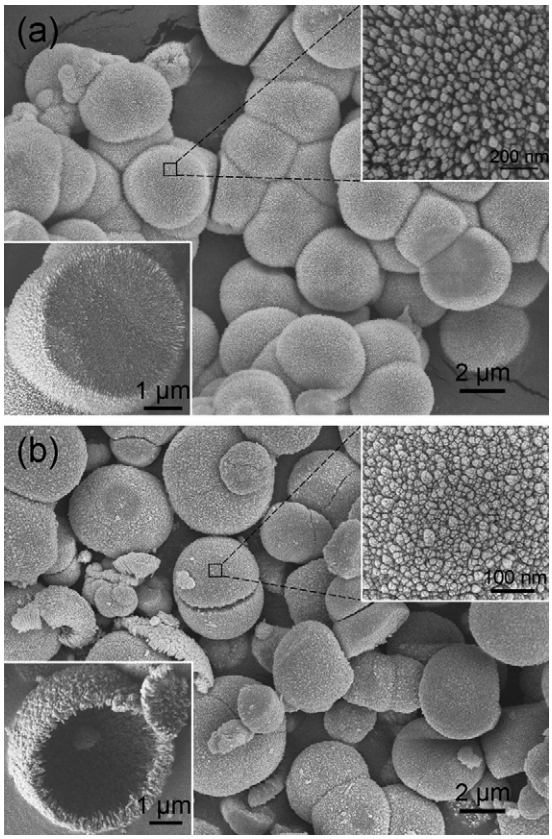

Fig. 7. FE-SEM images of the samples prepared at (a) 100 °C and (b) 140 °C for 24 h. Inset images show the corresponding images of a single microsphere.

When the reaction temperature was further increased to 140 °C, the main structures of the hollow spheres were similar to that when prepared at 120 °C (Fig. 7b), while the outer layer became thinner and the subunits grew larger (inset in Fig. 7b). This phenomenon could be interpreted since the Ostwald ripening would be more efficient at higher temperatures. In combination with the above XRD results, it is confirmed that CuO solid sphere, CuO hollow sphere, and CuO/Cu_2O hollow sphere were formed after reaction at temperatures of 100, 120, and 140 °C for 24 h.

Electrochemical performance of CuO hollow sphere was evaluated by galvanostatic charge/discharge cycling at a current density of 67 mA g^{-1} (0.1*C*), as shown in Fig. 8. For comparison, the electrochemical properties for CuO solid sphere and CuO/Cu_2O hollow sphere measured under the same electrochemical conditions were also provided. Fig. 8 shows the charge/discharge profiles of these electrodes in the 1st, 5th, 10th, and 20th cycles. In the first discharge step, all electrodes presented a long voltage plateau at about 1.2 V and a short voltage plateau at about 0.9 V, followed by a tilt curve down to the cutoff voltage of 0.01 V, which are typical characteristics of voltage trends for CuO electrodes [8,9]. The first discharge and charge capacities are 971 and 606 mAh g^{-1} for CuO hollow sphere, 909 and 535 mAh g^{-1} for CuO solid sphere, and 1016 and 638 mAh g^{-1} for CuO/Cu_2O hollow sphere composite electrodes. Compared to the theoretical capacity of CuO (670 mAh g^{-1}) and Cu_2O (375 mAh g^{-1}), the extra discharge capacity of all three anodes is generally attributed to surface phenomena such as the decomposition of electrolyte accompanying the formation of the solid electrolyte interface (SEI) layer, possibly interfacial lithium storage [30], as well as efficient transport of lithium ions granted by the hierarchical superstructures. The initial capacity loss may result from the incomplete conversion reaction and irreversible lithium loss due to the formation of SEI layer [31–33].

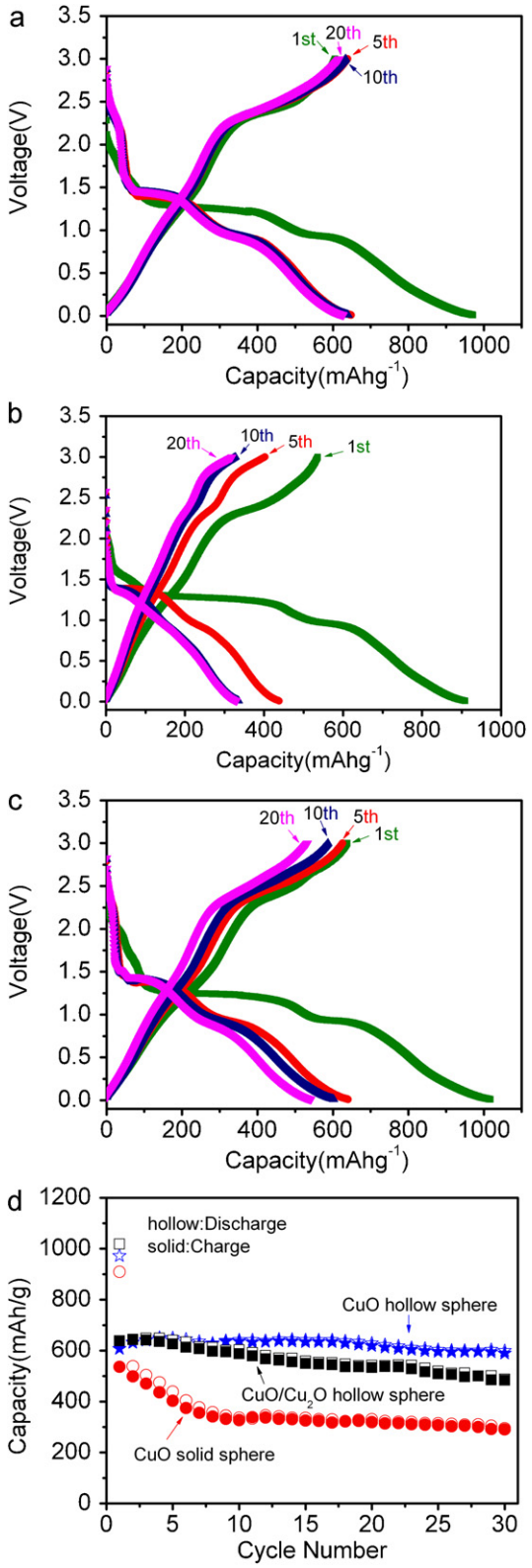

Fig. 8. Galvanostatic charge–discharge curves for (a) CuO hollow sphere, (b) CuO solid sphere, and (c) CuO/Cu_2O hollow sphere after 1st, 5th, 10th, and 20th cycles between 3 and 0.01 V at a current density of 67 mA g^{-1} (0.1*C*), and (d) comparison of the cycling performance of CuO hollow sphere, CuO solid sphere, and the CuO/Cu_2O hollow sphere.

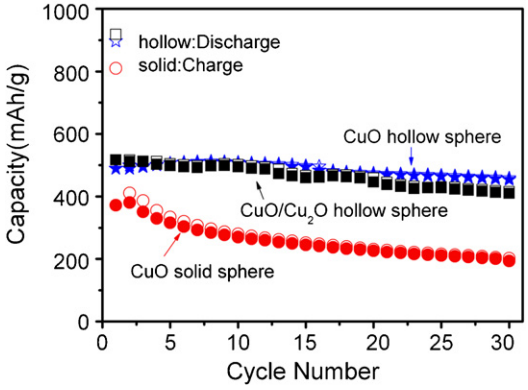

Fig. 9. Cycling performances of CuO solid sphere, CuO hollow sphere, and CuO/Cu_2O hollow sphere at a current density of 670 mA g^{-1} (1*C*).

Though the initial discharge capacity and Coulombic efficiency of CuO hollow sphere are not the best among three electrodes, the CuO hollow sphere electrode presents much better electrochemical lithium storage performance than CuO solid sphere since the second cycle. After five discharge/charge cycles, a higher reversible capacity of about 650 mAh g^{-1} than CuO/Cu_2O hollow sphere was obtained. The Coulombic efficiency rapidly rose from 62.4% in the first cycle to 98.4% in the fifth one and then remained above 98% in the following cycles (Fig. 8a). In contrast, the reversible capacity of the CuO solid sphere electrode rapidly dropped to 438 mAh g^{-1} with a low Coulombic efficiency of 91.7% after the fifth cycle and then the reversible capacity decreased to 319 mAh g^{-1} with an increased Coulombic efficiency of 96.7% for the 20th cycle (Fig. 8b). Comparing with CuO hollow sphere electrode, the CuO/Cu_2O composite electrode showed a larger discharge/charge capacity in the first cycle but suffered from the fast reversible capacity fading (i.e., 625 mAh g^{-1} for the fifth cycle, 532 mAh g^{-1} for the 20th cycle, as shown in Fig. 8c). More importantly, CuO hollow sphere exhibited a much better cycling performance than CuO solid sphere or CuO/Cu_2O hollow sphere (Fig. 8d). It is thus seen that the reversible capacity of CuO solid sphere and CuO/Cu_2O hollow sphere decreased from 535 mAh g^{-1} to 290 mAh g^{-1} and from 638 mAh g^{-1} to 483 mAh g^{-1}, respectively, upon 30 cycles. In contrast, the reversible capacity of CuO hollow sphere remained at 598 mAh g^{-1} after 30 cycles.

The comparative studies indicate that the reversible capacity of 598 mAh g^{-1} for CuO hollow sphere is much better than those previously reported, such as 296 mAh g^{-1} for CuO nanomicrospheres [2], 300 mAh g^{-1} for hierarchical CuO micro/nanostructures [5], 450 mAh g^{-1} for carbon nanotube/CuO [2], or even 550 mAh g^{-1} for CuO nanoribbons [34]. The initial Coulombic efficiency is 62.4% for CuO hollow sphere, which is higher than those of 45.2% for hierarchical CuO micro/nanostructures [5], 52.3% for carbon nanotube/CuO [2], 53.1% for CuO nanomicrospheres [2], or even 57.2% for CuO nanoribbons [34]. The most striking is that a Coulombic efficiency larger than 98% was observed after the fifth cycle, which indicates a high charge/discharge reversibility for the CuO hollow sphere electrode.

Cycling performance at a higher current density, an important parameter for PHEV and EV [35], was also measured for all electrodes. As shown in Fig. 9, CuO hollow sphere electrode exhibited a much better electrochemical performance compared to the CuO solid sphere or CuO/Cu_2O hollow sphere at a high current rate of 670 mA g^{-1} (1*C*). After 30 cycles, the reversible capacity of CuO solid sphere rapidly dropped from 373 to 193 mAh g^{-1}, while CuO/Cu_2O hollow sphere only delivered a reversible capacity of 409 mAh g^{-1}. Comparatively, CuO hollow sphere still delivered a reversible capacity of 457 mAh g^{-1} with a high Coulumbic effi-

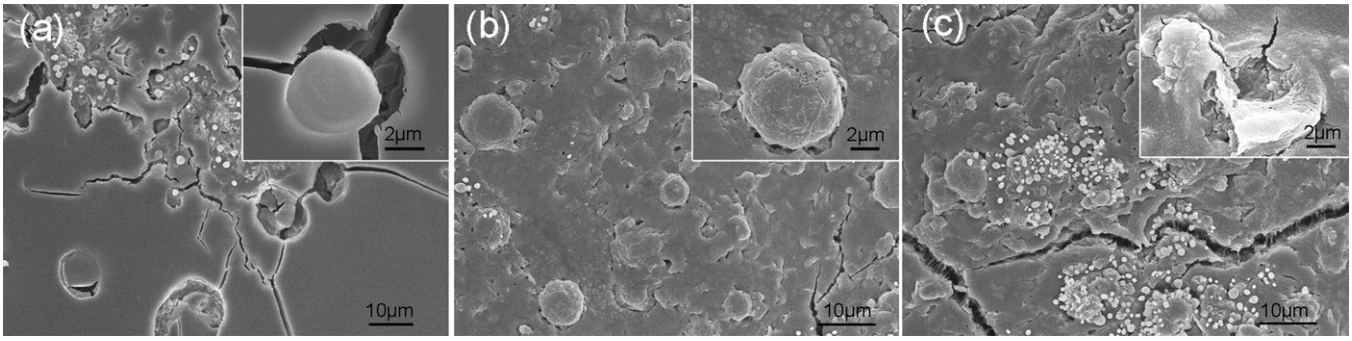

Fig. 10. FE-SEM images of (a) solid CuO sphere, (b) hollow CuO sphere, and (c) hollow CuO/Cu_2O sphere after 30 cycles. Inset images show the corresponding images of a single sphere.

ciency of 99% after the 30th cycle, which is much higher than the theoretical capacity of graphite of 372 mAh g^{-1}. Such a high capacity could be among the best reported values for all CuO-based electrodes tested under the similar conditions.

Because of the merits of highly reversible capacity, excellent cyclic performance, and high couloumbic efficiency, CuO hollow microspheres were believed to be a good candidate as anode material of high-performance lithium ion batteries. The superior Li-battery performance for CuO hollow microspheres may be due to two factors: (1) the nano/microstructure may contribute to the improved electrochemical performance towards lithium storage, while the microscopic structure guarantees the integrity of particles as well as quick infiltration of electrolyte. The oriented self-assembly of nanorods may ensure that most CuO building blocks participate in the electrochemical reactions and thus provide large electrode/electrolyte contact areas, leading to a short diffusion length and an enhanced electronic conductivity necessary for higher capacity; and (2) by taking into account the difference between the CuO initial molar volume and the molar volume of the fully theoretical lithiated phase (CuO converts to Cu and Li_2O), the volume change during Li uptake, ΔV_m, can be calculated to be around 80% as follows:

$$\Delta V_m = \frac{V_m(\mathrm{Cu}) + V_m(\mathrm{Li_2O}) - V_m(\mathrm{CuO})}{V_m(\mathrm{CuO})} \quad (3)$$

$$V_m = \frac{N_A . V_{\mathrm{UC}}}{Z} \quad (4)$$

where N_A is Avogadro's Number, V_{UC} is volume of the unit cell (V_{UC}(Cu) = 47.24 Å^3, V_{UC}(Li_2O) = 98.55 Å^3, and V_{UC}(CuO) = 81.03 Å^3), and Z is the number of formula units in the unit cell. The large volume change can be accommodated by the nanoscale interspaces between nanorods and the hollow interiors in CuO microspheres which can be considered as an elastic buffer, and thus the strain associated with the volume variations during Li uptake–release can be relieved, accounting for the good cycle performance.

These results may lead to important implications in designing new high-performance lithium ion batteries materials. Namely, a suitable void space is highly useful for improving the electrochemical performance. This assumption is further verified by different cyclic behaviors of the microspheres with different hollow interiors. As can be seen from Figs. 8d and 9, CuO hollow sphere exhibited a most stable cyclic performance among all three samples. In contrast, CuO solid sphere without hollow interiors exhibited a quick decrease in capacity for the first several cycles; while CuO/Cu_2O hollow sphere with largest hollow interiors exhibited a gradual decrease in capacity extends up to the 30th cycle. This discrepancy may be closely related to the different interior structures. A solid interior cannot provide enough void space to buffer the volume expansion, leading to the destruction of the electrodes and electrochemical performance worsening, while overlarge hollow interior is also harmful to the structural stability since the hollow structure may be metastable and not robust enough to prevent its breaking during the Li uptake–release. In addition, overlarge hollow interior is unfavorable for high volumetric specific capacity. FE-SEM characterizations of all three samples after 30 cycles support the above hypothesis well, as shown in Fig. 10. Most of CuO hollow microspheres maintained the shape integrity after 30 cycles (Fig. 10b). In contrast, most of CuO solid spheres were destroyed and even peeled off from the electrodes, leaving some holes in the surface of electrodes (Fig. 10a); while CuO/Cu_2O hollow spheres were exploded and many small particles were observed after 30 cycles (Fig. 10c). It is apparent that high structural stability leads to the excellent cycling performance of hollow CuO sphere.

4. Conclusion

A facile green synthetic route is demonstrated to construct CuO hierarchical microspheres with hollow interiors assembled by nanorods. Time-dependent experimental results illustrated that these CuO hierarchical microspheres were formed through a combined process of self-assembly and Ostwald's ripening. Depending on the reaction condition, hierarchical spheres were tuned to show different morphologies and microstructures. When explored as the electrode materials for lithium ion batteries, these CuO hollow microspheres exhibited good cycle performance and enhanced lithium storage capacity. This superior Li-battery performance resulted from the synergetic effect of small diffusion lengths in nanorod building blocks and proper void space to buffer the volume expansion. Considering the cost-effective synthesis and the merits of hollow microspheres in improving electrochemical performance, we believe that the results reported in this work might provide some new insights into the morphology-controllable design of high-performance anode materials for next-generation lithium ion batteries.

Acknowledgements

This work was financially supported by NSFC under the contract (Nos. 20773132, 20771101, 20831004, and 20903097), National Basic Research Program of China (2009CB939801, 2011CB935904), the key project in the NSTPP (No. 2009BAE89B00), FIPYT (Nos. 2009HZ0004-1 and 2008F3116) and FJIRSM fund (Nos. SZD-09002-3, SZD09003-1, and 2010KL002).

References

[1] J.Y. Kim, J.C. Park, H. Kang, H. Song, K.H. Park, Chem. Commun. 46 (2010) 439.
[2] S.F. Zheng, J.S. Hu, L.S. Zhong, W.G. Song, L.J. Wan, G.Y. Guo, Chem. Mater. 20 (2008) 3617.
[3] J. Xu, D. Xue, J. Phys. Chem. B 109 (2005) 17157.
[4] R.V. Kumar, Y. Diamant, A. Gedanken, Chem. Mater. 12 (2000) 2301.

[5] S.Y. Gao, S.X. Yang, J. Shu, S.X. Zhang, Z.D. Li, K. Jiang, J. Phys. Chem. C 112 (2008) 19324.
[6] S. Venkatachalam, H.W. Zhu, C. Masarapu, K.H. Huang, Z. Liu, K. Suenaga, B.Q. Wei, ACS Nano 3 (8) (2009) 2177.
[7] J.Y. Xiang, J.P. Tu, L. Zhang, Y. Zhou, X.L. Wang, S.J. Shi, J. Power Sources 195 (2010) 313.
[8] S. Grugeon, S. Laruelle, R. Herrera-Urbina, L. Dupont, P. Poizot, J.M. Tarascon, J. Electrochem. Soc. 148 (2001) A285.
[9] E.A. Souza, R. Landers, L.P. Cardoso, T.G.S. Cruz, M.H. Tabacnikes, A. Gorenstein, J. Power Sources 155 (2006) 358.
[10] X.J. Zhang, D.G. Zhang, X.M. Ni, J.M. Song, H.G. Zheng, J. Nanopart. Res. 10 (2008) 839.
[11] L.B. Chen, N. Lu, C.M. Xu, H.C. Yu, T.H. Wang, Electrochim. Acta 54 (2009) 4198.
[12] X.P. Gao, J.L. Bao, G.L. Pan, H.Y. Zhu, P.X. Huang, F. Wu, D.Y. Song, J. Phys. Chem. B 108 (2004) 5547.
[13] J. Zhu, X.F. Qian, J Solid State Chem. 183 (2010) 1632.
[14] J.C. Park, J. Kim, H. Kwon, H. Song, Adv. Mater. 21 (2009) 803.
[15] S.Q. Wang, J.Y. Zhang, C.H. Chen, Scripta Mater. 57 (2007) 337.
[16] P. Poizot, S. Laruelle, S. Grugeon, L. Dupont, J.M. Tarascon, Nature 407 (2000) 496.
[17] X. Wang, X.L. Wu, Y.G. Guo, Y.T. Zhong, X.Q. Cao, Y. Ma, J.N. Yao, Adv. Funct. Mater. 20 (2010) 1680.
[18] R. Demir-Cakan, Y.S. Hu, A. Markus, M. Joachim, T. Maria-Magdalena, Chem. Mater. 20 (2008) 1227.
[19] K. Hyesun, C. Jaephil, Chem. Mater. 20 (2008) 1679.
[20] U. Lafont, S. Waichman, M. Valvo, E.M. Kelder, J. NanoSci. Nanotechnol. 10 (7) (2010) 4273.
[21] X.W. Lou, L.A. Archer, Z. Yang, Adv. Mater. 20 (2008) 3987.
[22] A.M. Cao, J.S. Hu, H.P. Liang, L.J. Wan, Angew. Chem. Int. Ed. 44 (2005) 4391.
[23] J.Z. Yin, Q.Y. Lu, Z.N. Yu, J.J. Wang, H. Pang, F. Gao, Cryst. Growth Des. 10 (2010) 40.
[24] X.M. Yin, C.C. Li, M. Zhang, Q.Y. Hao, S. Liu, L.B. Chen, T.H. Wang, J. Phys. Chem. C 114 (2010) 8084.
[25] B. Liu, H.C. Zeng, J. Am. Chem. Soc. 126 (2004) 8124.
[26] S.H. Liu, R.M. Xing, F. Lu, R.K. Rana, J.J. Zhu, J. Phys. Chem. C 50 (2009) 21042.
[27] Y.S. Luo, X.J. Dai, W.D. Zhang, Y. Yang, C.Q. Sun, S.Y. Fu, Dalton Trans. 39 (2010) 2226.
[28] H.G. Yang, H.C. Zeng, J. Phys. Chem. B 108 (2004) 3492.
[29] G. Petra, F. Vojmir, L. Christian, M. Jadran, Acta Chim. Slov. 51 (2004) 203.
[30] J. Maier, Nature Mater. 4 (2005) 805.
[31] S. Laruelle, S. Grugeon, P. Poizot, M. Dolle, L. Dupont, J.M. Tarascon, J. Electrochem. Soc. 149 (2002) A627.
[32] G. Sudant, E. Baudrin, D. Larcher, J.M. Tarascon, J. Mater. Chem. 15 (2005) 1263.
[33] J. Liu, H. Xia, L. Lu, D.F. Xue, J. Mater. Chem. 20 (2010) 1506.
[34] F.S. Ke, L. Huang, G.Z. Wei, L.J. Xue, J.T. Li, B. Zhang, S.R. Chen, X.Y. Fan, S.G. Sun, Electrochim. Acta 54 (2009) 5825.
[35] M. Armand, J.M. Tarascon, Nature 451 (2008) 652.